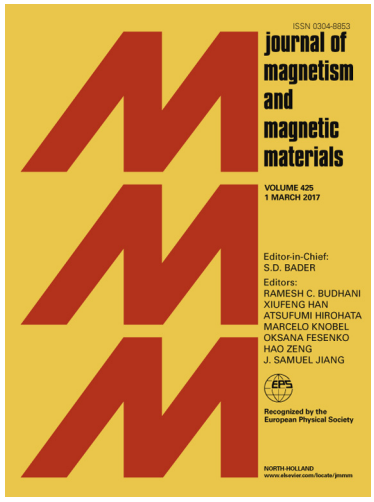

Research articles

Typical experiment vs. in-cell like conditions in magnetic hyperthermia: effects of media viscosity and agglomeration

I.J. Bruvera, D.G. Actis, M.P. Calatayud, P. Mendoza Zélis

PII: S0304-8853(19)31051-0
DOI: https://doi.org/10.1016/j.jmmm.2019.165563
Article Number: 165563
Reference: MAGMA 165563

To appear in: *Journal of Magnetism and Magnetic Materials*

Received Date: 26 March 2019
Accepted Date: 11 July 2019

Please cite this article as: I.J. Bruvera, D.G. Actis, M.P. Calatayud, P. Mendoza Zélis, Typical experiment vs. in-cell like conditions in magnetic hyperthermia: effects of media viscosity and agglomeration, *Journal of Magnetism and Magnetic Materials* (2019), doi: https://doi.org/10.1016/j.jmmm.2019.165563

Typical experiment vs. in-cell like conditions in magnetic hyperthermia: effects of media viscosity and agglomeration

I.J. Bruvera[a], D.G. Actis[a], M.P. Calatayud[b,c], P. Mendoza Zélis[a]

[a] *Instituto de Física La Plata (IFLP-CONICET), Departamento de Física, Facultad de Ciencias Exactas, Universidad Nacional de La Plata (UNLP), c.c. 67, 1900 La Plata, Argentina*

[b] *Aragon Institute of Nanoscience (INA), University of Zaragoza, 50018 Zaragoza, Spain*

[c] *Condensed Matter Physics Department, Science Faculty, University of Zaragoza, 50009 Zaragoza, Spain*

Abstract

Magnetic nanoparticles (MNPs) can be used to transform electromagnetic energy into heat in hyperthermic treatment of cancer and other thermally activated therapies. The MNPs heating efficiency depends strongly on the combination of the MNPs' structural properties and environmental conditions. MNPs hyperthermic yield is usually studied in diluted suspensions, although, in the actual therapy, the particles end mostly aggregated and fixed into cellular structures.

In this work, the heating efficiency of low size dispersion Fe_3O_4 MNPs, defined as the Specific Absorption Rate (SAR), was studied in two conditions: liquid suspension (ferrofluid FF, typical characterization state) and gel matrix (ferrogel FG, mimicking biological application environment). The samples were characterized by TEM, ZFC-FC and SAXS. Their magnetic response to radio-frequency fields was measured by induction in order to obtain SAR values from the magnetization cycles area. 3D maps of SAR versus field amplitude and frequency were elaborated in order to compare the response of fixed and suspended MNPs. Structural characterization shows FG's MNPs agglomerated in a crystal-like mesostructure with a well defined interparticle distance. SAR results show a clear difference of behaviour between liquid and gel matrices, with larger SAR values for the FG sample indicating a lower

Email address: pmendoza@fisica.unlp.edu.ar (P. Mendoza Zélis)

resonance frequency, inside the studied region, for fixed MNP. Additionally, the local maximum suggested in FGs SAR map indicates a behaviour outside linear response regimen as expected for the applied field amplitudes.

Keywords: Specific Absorption Rate, Magnetic nanoparticles, Magnetic Hyperthermia

1. Introduction

Magnetic nanoparticles (MNPs) are being extensively studied for their applications in biomedicine.[1] In cancer treatment, the MNPs are used as a heating agent for thermoablation and magnetic fluid hyperthermia.[2] In these therapies, the particles are introduced inside the tumor and the region is exposed to a radio-frequency electromagnetic field (RF) with frequencies around 100 kHz and amplitudes up to 15 kA/m.[3] The MNPs absorb energy from the field and release it to their surroundings as heat, producing thermal damage to the tumor.[4, 5] In order to deliver an adequate thermal dose, a key aspect for these therapies is a thorough and trustworthy knowledge of the MNPs heating efficiency. This efficiency is quantified by the Specific Absorption Rate (SAR) *i.e.* the amount of power the particles absorb from the field per unit mass. For a set of MNPs, the SAR value is not only determined by the particles properties, but also by the viscosity of the supporting medium, the interaction between particles, and the frequency f and amplitude H_0 of the applied field. So it is that two identical MNP assemblies supported in different media and exposed to the same RF could exhibit different SAR values. This effect has been studied by comparing the thermal dissipation for a single applied field frequency of MNPs supported in liquid with MNPs supported in hydrogel[6], glycerol[7] and gelatine[8], and for many frequencies in agar[9]. Also, it has been shown that MNPs are fixed rather strongly to the tumour tissue after injection into experimentally grown tumours in mice.[8] In all cases results indicate a noticeable diminution of the power dissipation for the fixated MNPs. This effect is generally attributed to the cancellation of Brown's dissipation mechanism although this cancellation will provoke a SAR diminution only for frequencies larger than the resonance frequency of the sample. In this direction, a recent publication by Cabrera et. al[10] suggests that the principal effect of the internalization of MNPs by living cells is due the increase in agglomeration rather than immobilization.

The typical method for SAR determination is the calorimetric measurement

of the power dissipation of MNPs in liquid suspension. This method provides a direct result from the temperature increase of the studied ferrofluid (FF) but presents several limitations for the characterization of solid and biological samples. In recent years an alternative method based on the inductive determination of the RF hysteresis loops has been developed by several research groups with very good results.[7, 10, 11, 12, 13, 14]

In this work, the SAR dependencies with H_0 and f of magnetite MNPs ferrofluid (FF) and ferrogel (FG) are studied using RF hysteresis loop area determination by induction measurements. This method allows to perform several measurements in a short time, so it was used to construct colour maps of SAR values versus field amplitude and field frequency by sweeping through several RF generator configurations. These maps are used to compare the performance of two samples that *a priori* differ only in their supporting media: the FF represents the typical and simplest media for studying MNPs, while the FG constitutes a high viscosity matrix where MNPs are fixed and usually present some degree of agglomeration. This fixed-agglomerated particle condition is similar to the final state of the MNPs in biological media after their incorporation by the cells as reported in [15].

2. Materials and methods

2.1. RF generation

The RF field is generated by a power source-resonator set *Hüttinger TIG 2,5/300* with a [30; 300] kHz nominal frequency range and a 2.5 kW maximum output. The resonator's RLC circuit can be configured with up to 4 parallel connected capacitors and an up to 4 turns internal inductance in series with the external working coil. A set of capacitors of different values allows to generate up to 80 resonance frequencies for every working coil. Each resonance frequency determines a maximum generated field proportional to the maximum circulating current.

The intensity of the working coil longitudinal field was measured for several generator intermediate DC currents (IDC) in function of the longitudinal position z inside the coil. The observed dependence was the expected for this 4 turn inductor, presenting a maximum field intensity of 55 mT in the center of the coil for the maximum IDC value (fig. 1).

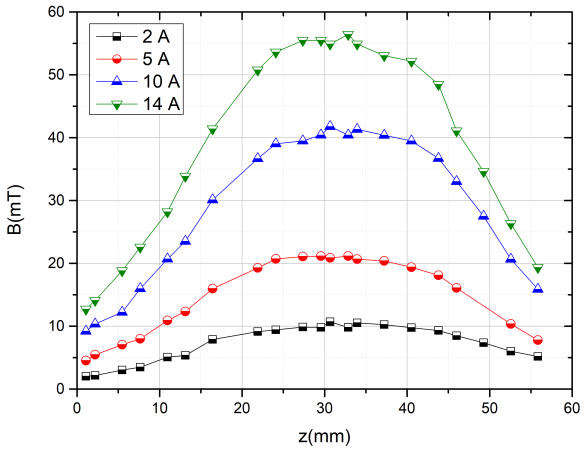

Figure 1: Magnetic induction intensity versus longitudinal position z in the working coil for several IDC values.

2.2. RF cycles measurement

In order to measure the magnetization M of the sample during the application of the RF field, an *ad hoc* device was constructed in a similar way to Bekovic and Mehdaoui[16, 17]. Two 10 turns, 5 mm radius, contrariwise-wounded pick-up coils c_s and c_f, connected in series were coaxially mounted on a plastic screw-like positioner with a fixed separation of 23 mm between them (fig. 2). 60 μm thick copper wire was used for the coils. The positioner fixes into a second plastic piece with an internal female thread. This second piece is attached to the working coil so the axial position of the pick-up coils can be precisely controlled by rotating the positioner.

The pick-up coils circuit is completed by a low pass RC filter with a 2 MHz cut-off frequency and a 5 GS/s oscilloscope (*Tektronix TDS 3012*). A third coil is placed around the external plastic piece to measure the time dependence of the applied field $H(t)$. The absolute instantaneous field value in the sample position is obtained from a previous calibration.

The coils output signal is conditioned and integrated numerically in order to obtain the RF loops area and then, the corresponding SAR values.

2.3. Sample preparation

Since no actual biological media is studied in this work, a non biocompatible organic based FF was used for the experiments. The utilized suspension

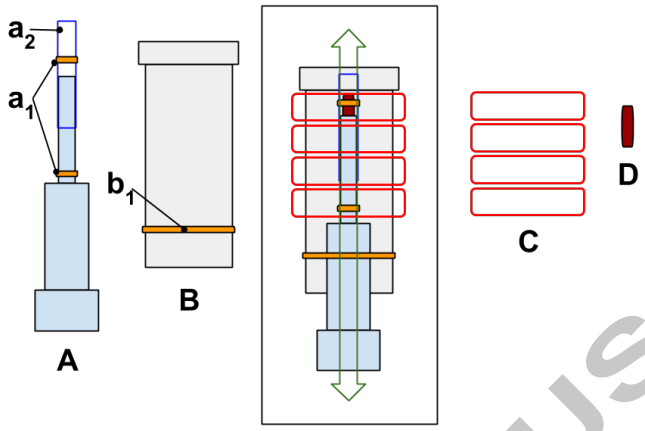

Figure 2: Inductive magnetization sensor. (A): central piece with the pick-up coils a_1 contrary wounded in series. Sample coil c_s is wounded on a plastic straw a_2. (B): external piece with internal female thread and applied field sensing coil b_1. A fits inside B and both fit inside the working coil C. Sample D is placed inside the top end of the plastic straw as shown in central picture.

presents several experimental advantages such as high stability, small size dispersion and light coating.

2.3.1. Synthesis

Magnetite nanoparticles were synthesized by high-temperature decomposition of 10 mmol of Fe(oleate) (procedure described here [18]) in the presence of 4 mmol of oleic acid and using 20 mL of trioctylamine and 80 mL of benzyl ether as mixed solvent (boiling point 295 °C). The reaction was refluxed for 1 hour under vigorous stirring and N_2 atmosphere. Then the particles were washed several times with hexane and ethanol. The final magnetite concentration of the suspension was 11.7(5) kg/m^3.

2.3.2. Ferrogel preparation

A ferrogel (FG) was elaborated from the same MNPs. 500(5) μL of the FF were mixed with 390(1) mg of melted commercial paraffin gel wax. A final magnetite concentration of 1.2 kg/m^3 was obtained. A portion of this sample was placed inside a gelatin capsule, filling it completely. Another identical capsule was filled with clean gel wax for background measurements.

2.4. Structural characterization

TEM images of a dry droplet of the FF were taken in a *FEI Tecnai T20, 200 kV*.
ZFC-FC experiments were performed on both, FF and FG samples at a 2.4 K/min rate and a 8 kA/m field.
SAXS measurements were performed using a *XEUSS 1.0* system from *XENOCS* equipped with a 2D photon counting pixel X-ray detector *Pilatus 100k (DECTRIS, Switzerland)*. The scattering intensity, $I(q)$, was recorded in the range of the momentum transfer $0.04 < q < 1.4\,\mathrm{nm}^1$, where $q = 4\pi sin(\theta)/\lambda$, with 2θ the scattering angle, and $\lambda = 0.15419\,\mathrm{nm}$ the weighted average of X-ray wavelength of the Cu $K_{\alpha 12}$ emission lines. All measurements were carried out using a quartz capillary as sample holder.

3. Results and discussion

3.1. TEM

TEM images show quasi-spherical, crystalline particles with a narrow Lognormal size distribution of 9.5 nm mean and 1.7 nm standard deviation (fig. 3). Clusters of MNPs were not detected in the images.
FF presents years-long stability in hexane suspension at 10 g/L concentration. The interparticle distance obtained from concentration and size dispersion indicates a separation larger than the 3 radius limit established for dipolar interaction[19].

3.2. ZFC-FC

The blocking temperature T_B distribution of each sample was obtained from the derivative of the ZFC-FC difference respect to temperature as reported in Bruvera et al. [20]. From the comparison between frozen FF and FG results it can be seen that FG T_B distribution is narrower and has its maximum at a lower temperature (fig. 4). This modification is compatible with an increase in dipolar interaction between MNPs in the FG in regard to FF as reported by Denardin et al. [21].

3.3. SAXS

A SAXS mesurement was performed on a FG sample in order to verify MNP aggregation. The scattering of the clean gel wax was also measured

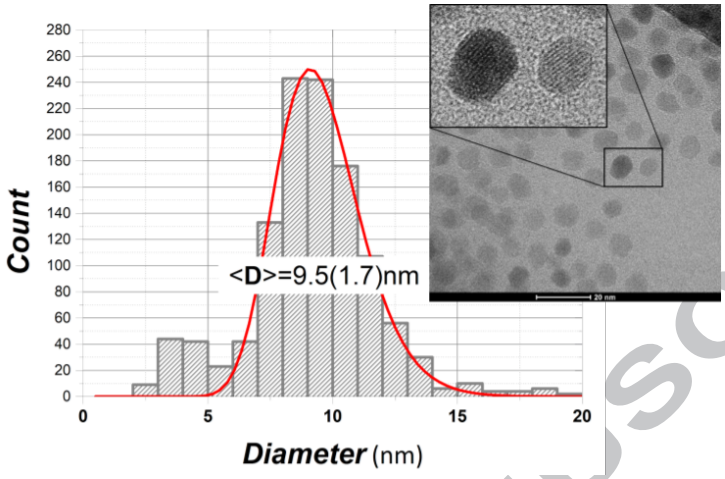

Figure 3: Size distribution from TEM images. Inset: TEM image example with a magnification showing the crystallinity of the particles. The fitting left out the smallest MNP with small incidence in volumetric magnetic response.

to distinguish its signal from the MNPs'. Figure 5 shows SAXS patterns for both FG sample and gel wax. The FG SAXS pattern presents two diffraction peaks in the positional ratio $1 : (4/3)^{1/2}$, corresponding to reflections [111] and [200] respectively of a face centered cubic (fcc) lattice (Fm3m symmetry). It is possible to calculate a cell parameter $a = 19.4(3)$ nm from the first order reflection at $q = 0.56(2)\,\mathrm{nm}^{-1}$. The cell parameter yields a distance between nearest neighbours $d = 13.7(2)$ nm. From this results, it can be inferred that nanoparticles in the FG were organized as a fcc mesostructure, a simple regular lattice that achieves the highest average density, with precisely defined interparticle spacing.

The consideration of all the structural information strongly suggests that, besides the immobilization in the gel matrix, the particles in the FG present also a considerable degree of agglomeration, possibly promoted by the lamellar molecular structure of the gel. The differences between FG's and frozen FF's T_B distribution, together with the regular interparticle distance arisen from SAXS results, constitute clear indications of MNP agglomeration in the gel matrix. On the other hand, the stability and concentration of the hexane FF, together with TEM images, indicates a mean interparticle distance of more than three diameters. This value is large enough to disregard dipolar interactions in the liquid suspension. In parallel with this, TEM results

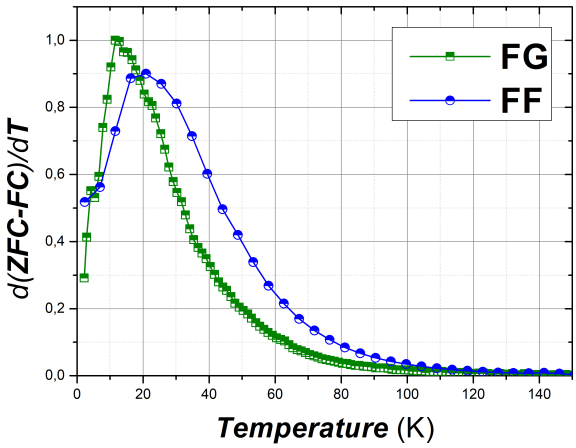

Figure 4: Blocking temperature distribution of FF and FG samples obtained from ZFC-FC experiments.

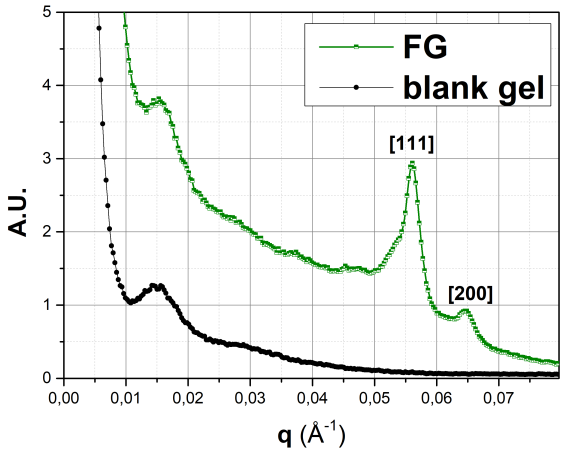

Figure 5: SAXS pattern of FG and clean gel wax samples. The nanoparticle organization in the FG sample is demonstrated by the presence of two diffraction peaks corresponding to reflections [111] and [200] of a face centered cubic lattice.

reported by Coral et al. [15] show MNPs agglomerated in endosomes after their incorporation by a cell culture. Thus, MNPs suspended in the gel matrix present a spatial distribution similar to those incorporated by cells and

rather different from the same particles in suspension.

3.4. SAR maps and RF cycles for FF and FG

A series of RF magnetization cycles measurements was conducted on both FG and FF samples in order to construct and compare specific power absorption SAR vs. RF-field-amplitude H vs. RF-field-frequency f maps. The practicality and speed of the inductive measurement system over the typical calorimetric method enables the realization of several experiments in a short time (less than 10 s per measurement) with little effect over the sample since temperature increase is less than 5 K for all measurements.
Figures 6 and 7 show SAR values maps for FF and FG samples subjected to several RF fields.
FF map shows a mostly monotonic increase in the direction of larger H and higher f with a maximum measured value of 94(5) W/g for [268.0(5) kHz; 48(1) kA/m].
FG map presents several differences with FF results. FG's SAR values are larger for every [f, H] point comparison between samples. The maximum value of 363(85) W/g was measured at maximum field amplitude, not for the higher 268.0(5) kHz frequency but for a lower one of 207.9(5) kHz. Moreover, SAR values at 260 kHz are higher than those at 268 kHz for all measured field amplitudes suggesting the presence of a local frequency maximum in the region that is not present in the FF map.

The use of the inductive SAR determination allows not only to obtain dissipation values but also to measure the actual magnetization cycles of the samples. Studying this cycles enables to a better understanding of the behavior showed in SAR maps. Figure 8 shows the comparison between FG and FF cycles at 268.0(5) kHz normalized by iron concentration. Susceptibility, maximum magnetization, remanence and cycle area are systematically smaller for FF while coercivity does not presents a well defined relation between samples. This cycle characteristics are similar for all the frequencies.

The differences between FF and FG cycles can be understood as an effect of two factors present in the FG: the agglomeration-driven dipolar interaction between nearby particles; and the cancelation of Brown's dissipation mechanism due to MNPs fixation. The effects of particle agglomeration on SAR may vary, as it has been shown that in the presence of dipolar interactions SAR is not a homogeneous function of MNPs concentration (i.e. inter-particle distance) [22, 23, 14]. Moreover, the cited work of Cabrera et al.

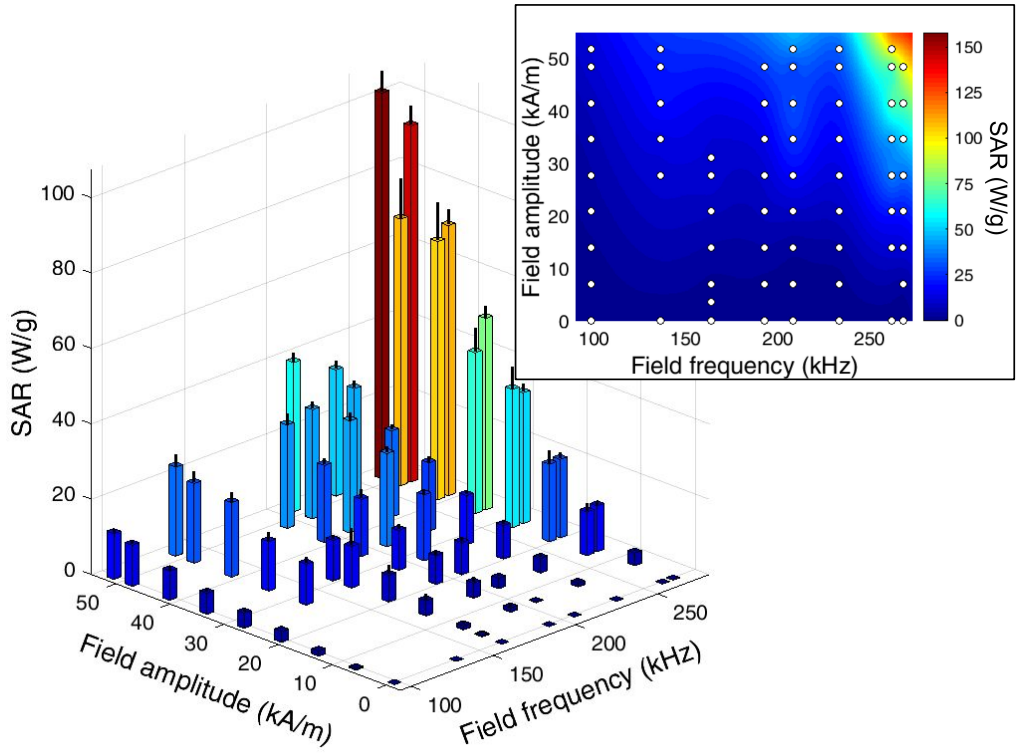

Figure 6: SAR values of FF sample. Bar position indicates applied field's amplitude and frequency. Bar height indicates mean SAR value from three measurements with black line at the top the standard deviation. Inset: colour map interpolated from SAR values. White dots mark the position of the 3D bars in the colour map.

[10] concludes that magnetic dipolar interactions, taking place within randomly ordered MNPs clusters, play a central role in the decrease of magnetic heating losses. In our case, the structural information indicates an agglomeration of MNPs with a well defined and compact spatial distribution that could be partially responsible of the measured increase in SAR values.[24] In parallel, as shown in the appendix, the absence of Browns mechanism leads to a longer relaxation time and a subsequently smaller, in this case inside the measurement range, resonance frequency between MNPs relaxation and the magnetic field. In addition, the presence of a local maximum is consistent with a behaviour outside linear response regime which is also evident from the non elliptical RF magnetization cycles measured at high field amplitudes.

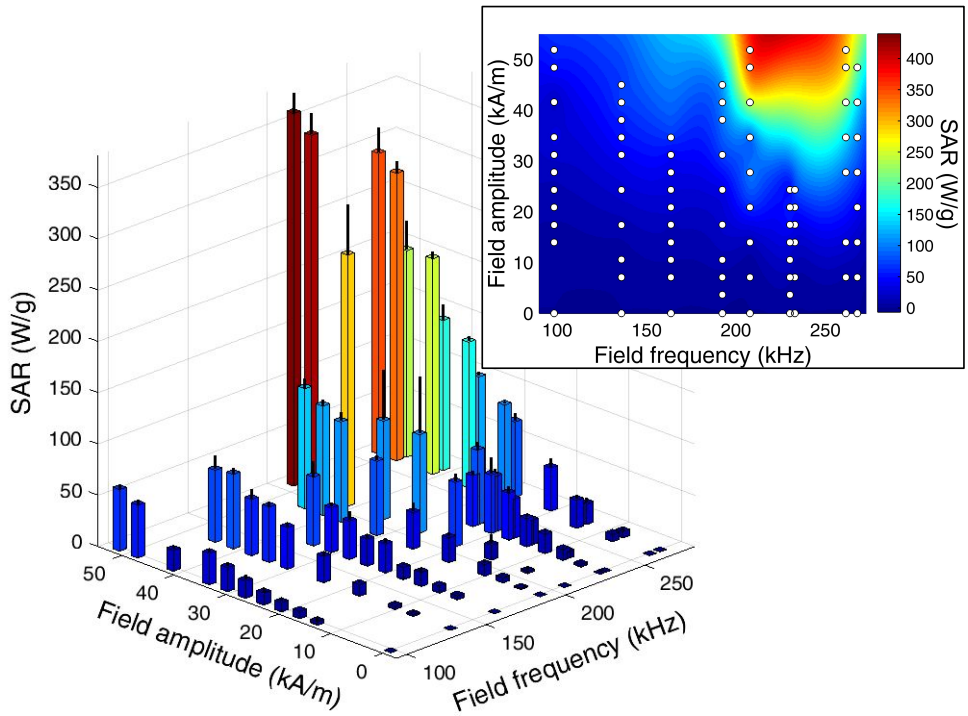

Figure 7: SAR values of FG sample. Bar position indicates applied field's amplitude and frequency. Bar height indicates mean SAR value from three measurements with black line at the top the standard deviation. Inset: colour map interpolated from SAR values. White dots mark the position of the 3D bars in the colour map.

4. Summary

An hexane ferrofluid (FF) and a paraffin ferrogel (FG) were prepared from the same batch of Fe_3O_4 nanoparticles (MNPs) in order to compare the power dissipation of the same MNPs in the FF typical characterization media with the response in the highly viscous, agglomerated, in-cell like conditions of the FG.

The specific absorption rate (SAR) landscapes of both samples were surveyed for a [98, 268] kHz x [0, 52] kA/m field-frequency x field-amplitude surface. Additionally, TEM, SAXS and SQuID measurements were performed on the samples in order to correlate structural characteristics with power absorption behavior.

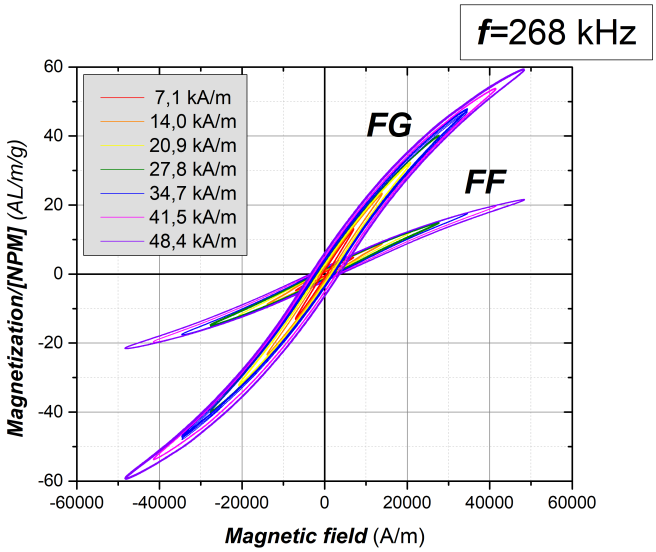

Figure 8: RF magnetization cycles comparison between FF and FG samples for the full field amplitude range at 268.0(5) kHz.

All the obtained structural information indicates that, while the MNPs in the FF stay in stable suspension with a mean interparticle distance larger than three diameters, the particles fixed in the FG are mostly agglomerated and separated by less than two diameters in a regular mesostructure. Because of this, dipolar interactions between particles should be negligible in the FF and considerable in the FG.

The comparison between both samples' hysteresis loops and SAR values shows a consistently larger power dissipation for the MNPs in the FG with a local SAR maximum in frequency that is not present in the FF's results. All this can be understood as the combined effect of the dipolar interactions and the cancellation of the Brown mechanism in the FG.

5. Conclusions

The difference between 9.5(1.7) nm diameter MNPs response suspended in hexane and fixed in paraffin gel to RF in the range [98, 268] kHz - [0, 52] kA/m has been proven. SAR values for MNPs in FG are consistently higher than in FF by a factor 2 or more. Additionally, the presence of a local SAR frequency maximum was detected only for FG.

The agglomeration of the MNPs in the FG matrix has been proven with a precise determination of the interparticle distance. This constitutes a condition much closer to the particles incorporated into cells than in the previously reported experiments where MNPs were homogeneously dispersed in FG matrix.
The SAR differences between FF and FG can be understood as an effect of the agglomeration-driven dipolar interaction between nearby particles and the cancelation of Brown‘s dissipation mechanism due to MNPs fixation. The ordered spatial distribution observed in the FG sample could be partially responsible for the increase in SAR values together with the absence of Browns mechanism that leads to a smaller, in this case inside of the measurement range, resonance frequency between MNPs relaxation and the magnetic field. Finally, inductive SAR determination has demonstrated to be a reliable and practical technique with several advantages over the calorimetric method. The possibility of *ex vivo* SAR determination of MNPs incorporated to biological samples is promising and will be tested soon.

Acknowledgements

The authors would like to acknowledge CONICET and UNLP of Argentina for financial support through Grant Nos. PIP 0720 and X11/680. The group would also like to thank Mr. Pablo Mereles for his continuous technical assistance and advice for our experiments and Dr. Marcelo Ceolín from INIFTA for his assistance with SAXS measurements.

Appendix A. MNPs power dissipation

In a linear response theory framework, the specific power absorbed by the MNPs from the field can be expressed as

$$p = \frac{\pi \mu_0^2 M_s^2 V H_0^2 f}{3kTn} \frac{\omega\tau}{1+(\omega\tau)^2}, \tag{A.1}$$

[25]

depending on thermal energy kT, material properties like saturation magnetization M_s, $mass/volume$ concentration n and MNP volume V, and RF parameters as amplitude H_0 and frequency f. The resonant factor $\omega\tau/(1+(\omega\tau)^2)$ is called frequency factor (Φ) and depends on the relation between the angular field frequency $\omega = 2\pi f$ and the relaxation time τ. For

small frequencies ($\omega << 1/\tau$) this factor is proportional to $\omega\tau$ so, the SAR is proportional to $\tau H_0 f^2$ by a factor independent of RF parameters :

$$\omega << 1/\tau \Rightarrow SAR \propto \tau H_0^2 f^2 \tag{A.2}$$

If a MNPs assembly is exposed to a constant magnetic field and then the field is removed, the total magnetization of the assembly decays exponentially with a characteristic time τ, whose expression depends on the relaxation mechanism. There are two relaxation mechanisms typically contemplated for monodomine MNPs:

The fluctuation of the magnetization between the two opposite orientations determined by the so called "easy axis" within the particle is known as Nèel mechanism. Its characteristic time is

$$\tau_N = \tau_0 e^{KV_M/kT}$$

where $\tau_0 = 10^{-9}$ s, V_M is the particle's magnetic volume and K is the anisotropy constant.
If the MNPs are suspended in a fluid media, the relaxation can be achieved by the rotation of the particle itself. In this case, the characteristic Brown time is determined by the fluid viscosity η, the MNP hydrodynamic volume V_H and the thermal energy kT

$$\tau_B = \frac{3\eta V_H}{kT}$$

If the two mechanisms are accessible, the effective relaxation time is a combination of both:

$$\frac{1}{\tau} = \frac{1}{\tau_B} + \frac{1}{\tau_N} \tag{A.3}$$

predominating the smaller time *i.e.* the fastest mechanism.[26] By determining the τ value, these very distinct mechanisms governed by particle volume, directly conditionate the response of a MNPs sample to the RF. It can be noticed that while the Nèel mechanism depends only on temperature and on the intrinsic properties of the MNP, K and V_M; the Brown mechanism is determined by temperature and a media property as is viscosity.

if the Brown mechanism is dominant at least in one of the media (fig. A.9).

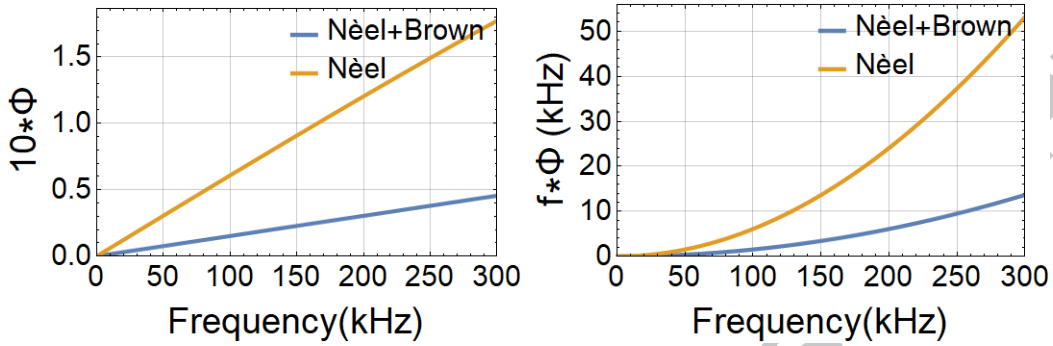

Figure A.9: Frequency factor $\Phi = \omega\tau/(1+(\omega\tau)^2)$ (left) and $f\Phi = \frac{SAR}{\pi\mu_0^2 M_s^2 V H_0^2} 3kTn$ (right) versus field frequency f for a MNP of diameter $D_M = D_H = 9.54$ nm and effective anisotropy constant $K_{ef} = 30\, kJ/m^3$ suspended in hexane, $\eta = 0.28\times10^{-3}\, Pa\, s$ at $T = 303$ K.

References

[1] Q. Pankhurst, N. Thanh, S. Jones, J. Dobson, Progress in applications of magnetic nanoparticles in biomedicine, Journal of Physics D: Applied Physics 42 (2009) 224001.

[2] A. B. Salunkhe, V. M. Khot, S. Pawar, Magnetic hyperthermia with magnetic nanoparticles: a status review, Current topics in medicinal chemistry 14 (2014) 572–594.

[3] K. Maier-Hauff, F. Ulrich, D. Nestler, H. Niehoff, P. Wust, B. Thiesen, H. Orawa, V. Budach, A. Jordan, Efficacy and safety of intratumoral thermotherapy using magnetic iron-oxide nanoparticles combined with external beam radiotherapy on patients with recurrent glioblastoma multiforme, Journal of Neuro-Oncology 103 (2011) 317–324.

[4] S. Dutz, R. Hergt, Magnetic particle hyperthermia: A promising tumour therapy?, Nanotechnology 25 (2014) 452001.

[5] M. Falk, R. Issels, Hyperthermia in oncology, International Journal of Hyperthermia 17 (2001) 1–18.

[6] U. M. Engelmann, J. Seifert, B. Mues, S. Roitsch, C. Menager, A. M. Schmidt, I. Slabu, Heating efficiency of magnetic nanoparticles decreases

with gradual immobilization in hydrogels, Journal of Magnetism and Magnetic Materials 471 (2019) 486 – 494.

[7] D. Cabrera, A. Lak, T. Yoshida, M. E. Materia, D. Ortega, F. Ludwig, P. Guardia, A. Sathya, T. Pellegrino, F. J. Teran, Unraveling viscosity effects on the hysteresis losses of magnetic nanocubes, Nanoscale 9 (2017) 5094–5101.

[8] S. Dutz, M. Kettering, I. Hilger, R. Mller, M. Zeisberger, Magnetic multicore nanoparticles for hyperthermia—influence of particle immobilization in tumour tissue on magnetic properties, Nanotechnology 22 (2011) 265102.

[9] M. Avolio, A. Guerrini, F. Brero, C. Innocenti, C. Sangregorio, M. Cobianchi, M. Mariani, F. Orsini, P. Arosio, A. Lascialfari, In-gel study of the effect of magnetic nanoparticles immobilization on their heating efficiency for application in magnetic fluid hyperthermia, Journal of Magnetism and Magnetic Materials 471 (2019) 504 – 512.

[10] D. Cabrera, A. Coene, J. Leliaert, E. J. Arts-Ibez, L. Dupr, N. D. Telling, F. J. Teran, Dynamical magnetic response of iron oxide nanoparticles inside live cells, ACS Nano 12 (2018) 2741–2752. PMID: 29508990.

[11] E. Garaio, J. Collantes, J. Garcia, F. Plazaola, S. Mornet, F. Couillaud, O. Sandre, A wide-frequency range ac magnetometer to measure the specific absorption rate in nanoparticles for magnetic hyperthermia, Journal of Magnetism and Magnetic Materials 368 (2014) 432 – 437.

[12] Z. Nemati, J. Alonso, I. Rodrigo, R. Das, E. Garaio, J. . Garca, I. Orue, M.-H. Phan, H. Srikanth, Improving the heating efficiency of iron oxide nanoparticles by tuning their shape and size, The Journal of Physical Chemistry C 122 (2018) 2367–2381.

[13] I. Morales, R. Costo, N. Mille, G. B. d. Silva, J. Carrey, A. Hernando, P. d. l. Presa, High frequency hysteresis losses on γ-fe2o3 and fe3o4: Susceptibility as a magnetic stamp for chain formation, Nanomaterials 8 (2018) 970.

[14] J. G. Ovejero, D. Cabrera, J. Carrey, T. Valdivielso, G. Salas, F. J. Teran, Effects of inter-and intra-aggregate magnetic dipolar interactions

on the magnetic heating efficiency of iron oxide nanoparticles, Physical Chemistry Chemical Physics 18 (2016) 10954–10963.

[15] D. F. Coral, P. A. Soto, V. Blank, A. Veiga, E. Spinelli, S. Gonzalez, G. Saracco, M. Bab, D. Muraca, P. C. Setton-Avruj, et al., Nanoclusters of crystallographically aligned nanoparticles for magnetic thermotherapy: aqueous ferrofluid, agarose phantoms and ex vivo melanoma tumour assessment, Nanoscale 10 (2018) 21262–21274.

[16] M. Beković, M. Trlep, M. Jesenik, V. Goričan, A. Hamler, An experimental study of magnetic-field and temperature dependence on magnetic fluids heating power, Journal of Magnetism and Magnetic Materials 331 (2013) 264–268.

[17] B. Mehdaoui, J. Carrey, M. Stadler, A. Cornejo, C. Nayral, F. Delpech, B. Chaudret, M. Respaud, Influence of a transverse static magnetic field on the magnetic hyperthermia properties and high-frequency hysteresis loops of ferromagnetic feco nanoparticles, Applied Physics Letters 100 (2012) 052403.

[18] A. Shavel, L. M. Liz-Marzán, Shape control of iron oxide nanoparticles, Physical Chemistry Chemical Physics 11 (2009) 3762–3766.

[19] F. H. Sánchez, P. M. Zélis, M. Arciniegas, G. A. Pasquevich, M. F. Van Raap, Dipolar interaction and demagnetizing effects in magnetic nanoparticle dispersions: Introducing the mean-field interacting superparamagnet model, Physical Review B 95 (2017) 134421.

[20] I. Bruvera, P. Mendoza Zélis, M. Pilar Calatayud, G. F. Goya, F. H. Sánchez, Determination of the blocking temperature of magnetic nanoparticles: The good, the bad, and the ugly, Journal of Applied Physics 118 (2015) 184304.

[21] J. Denardin, A. Brandl, M. Knobel, P. Panissod, A. Pakhomov, H. Liu, X. Zhang, Thermoremanence and zero-field-cooled/field-cooled magnetization study of co x (sio 2) 1- x granular films, Physical Review B 65 (2002) 064422.

[22] D. F. Coral, P. Mendoza Zelis, M. Marciello, M. d. P. Morales, A. Craievich, F. H. Sanchez, M. B. Fernandez van Raap, Effect of

nanoclustering and dipolar interactions in heat generation for magnetic hyperthermia, Langmuir 32 (2016) 1201–1213.

[23] I. Conde-Leboran, D. Baldomir, C. Martinez-Boubeta, O. Chubykalo-Fesenko, M. del Puerto Morales, G. Salas, D. Cabrera, J. Camarero, F. J. Teran, D. Serantes, A single picture explains diversity of hyperthermia response of magnetic nanoparticles, The Journal of Physical Chemistry C 119 (2015) 15698–15706.

[24] O. Hovorka, Thermal activation in statistical clusters of magnetic nanoparticles, Journal of Physics D: Applied Physics 50 (2017) 044004.

[25] R. E. Rosensweig, Heating magnetic fluid with alternating magnetic field, Journal of Magnetism and Magnetic Materials 252 (2002) 370–374.

[26] Q. A. Pankhurst, J. Connolly, S. Jones, J. Dobson, Applications of magnetic nanoparticles in biomedicine, Journal of physics D: Applied physics 36 (2003) R167.